Journal of Materials Chemistry B

Accepted Manuscript

ROYAL SOCIETY OF CHEMISTRY

www.rsc.org/materialsB

Journal of Materials Chemistry B

ARTICLE

The relationship between microstructure and *in vivo* degradation of modified bacterial cellulose sponges

C. Lai,[a,c] S.J.Zhang[b], .L. Q.Wang[a] , L.Y .Sheng[a] , Q. Z. Zhou[a] and T.F. Xi[a*]

Received 00th January 20xx,
Accepted 00th January 20xx

DOI: 10.1039/x0xx00000x

www.rsc.org/

Bacterial cellulose (BC) and hydroxyapatite (HA) possess unique structures and excellent biocompatibility. Considerable work has been performed to develop composites that promote bone repair. However, the use of BC/HA composites is limited because the lack of corresponding enzymes makes them non-degradable in vivo. In the present study, C6-carboxylated bacterial cellulose (TBC) was prepared in a bromide-free system. Several composite methods of TBC and HA are compared, including in situ formation, physical mixing and biomineralization. Composite sponges prepared by different methods were characterized by tensile testing, X-ray diffraction, Fourier transform infrared spectroscopy, scanning electron microscopy and in vivo degradation. The structural anisotropy of various sponges was analyzed to quantitatively evaluate their microstructure. The results suggest that the interaction between HA and TBC nanofibers has a large influence on microstructure and macroscopic properties. Moreover, the structural anisotropy and the speed of granulation ingrowth were strongly interdependent. This improved understanding of slowly degrading BC-based materials suggests that modified cellulose-based materials can be made degradable by altering their microstructure.

1.Introduction

Bone graft substitutes are used in the repair and reconstruction of bone tissue defects. Collagen and hydroxyapatite (HA) are the most popular materials in bone-repairing substitutes because their composites mimic the extracellular matrix (ECM) of natural bone. However, collagen/HA composites tend to crack under stress given the brittle nature of HA; additionally, their load-bearing property is not sufficient for use in bone grafts [1]. Collagen exhibits other significant drawbacks, such as its animal origin, cost and immunogenicity. Many materials have recently been investigated as a partial or complete replacement for collagen, including gelatin [2], poly(lactic-co-glycolic acid) [3], gellan [4] and chitosan [5]. As a polysaccharide, bacterial cellulose (BC) bears a strong resemblance to collagen in terms of its nanofibril architecture but does not exhibit immunologic reactivity. BC is a form of cellulose produced by bacteria, including Gluconacetobacter (also named Acetobacter), Acanthamoeba, Achromobacter, Zoogloea, and others [6]. As a cellulosic polymer, BC is a linear syndiotactic homopolymer composed of D-anhydroglucopyranose units (AGU), which are linked together by β-(1→4)-glycosidic bonds [7]. In contrast to native cellulose from plants, BC exhibits increased tensile

[a] *Shenzhen Key Laboratory of Human Tissue Regeneration and Repair, Shenzhen Institute, Peking University, Shenzhen 518057, China.*
[b] *Guangdong Key Laboratory of Orthopaedic Technology and Implant Materials, The First Affiliated Hospital of Guangzhou Medical university, Guangzhou 510120, China.*
[c] *National engineering research center for biomaterials, Sichun University, Chengdu 610064, China*
† Co-first author: Shujiang Zhang contributed equally to the manuscript and is also a co-first author.
* corresponding author

strength and a stiffness (in single fiber form) that is comparable to steel and Kevlar [8]. BC also exhibits numerous advantages, such as low cost, higher availability, nontoxicity and affinity to the polar reinforcing agents of HA given its hydrophilic characteristics, as described by the theory developed by Ciobanu [9]. In the field of bone regeneration, BC is capable of promoting the formation of calcium-deficient HA in a U.S. patent application [10] and in research reports [11, 12]. HA/BC composites can be obtained by various methods. Biomineralization is regularly observed in many studies [13,14] and involves soaking BC matrices in simulated body fluid with an ion concentration equivalent to that of human blood plasma at physiological pH and temperature. This method is analogous to natural bone precipitation. The physical mixing method often involves the mixing of aqueous suspensions of BC and engineered HA particles [15,16] whose interaction is primarily electrostatic [17]. In the in situ formation method, HA-BC composites are obtained by titrating Ca^{2+}, $PO4^{3-}$ and OH^{-} solutions into BC aqueous suspensions, forming nanoparticles on BC nanofibers [18].

However, the primary hydroxyl groups of cellulose do not exhibit sufficiently high reactivity to grow calcium phosphate crystals [19]. Interactions between Ca^{2+} ions and primary hydroxyl groups in water solutions are very weak and cannot compensate for entropy losses [17]. Additionally, the accessibility of the hydroxyl groups is reduced by multiple hydrogen bonds between the microfibers, which are tightly tangled. Thus, HA particles are not homogenously distributed throughout BC matrices. To enhance the nucleation of HA on the BC fibers, BC must be chemically modified to form ionized groups on the nanofibers. Our laboratory has developed techniques to modify BC to produce various derivatives [7,20]. Despite difficulties in the modification reaction, carboxylic functionalization can still occur at C6, the site of the primary hydroxyl group. The reactivity of BC carboxylate is considerably increased compared with cell-OH because the uniformity of accessibility has been enhanced in the form of BC carboxylate.

Another important reason for the modification of BC is to improve its bio-degradability in vivo. In tissue engineering applications, new tissue typically regenerates as the material degrades. However, cellulose is considered non-degradable because mammalian cells lack the molecular machinery to cleave the β-1,4 glycosidic bonds linking glucose residues in cellulose. The absence of degradation in mammalian systems has proved to be a major impediment to tissue substitution. Various approaches have been employed to make cellulose susceptible to degradation in vivo. Native cellulose consists of amorphous and crystalline parts, and degradation often occurs in the amorphous parts by hydrolysis of the b-1,4 glycosidic bond. By reducing the degree of crystallinity and enhancing enzyme accessibility, we might increase the chance of degradation in vivo. Some oxidants tend to exclusively react with amorphous regions and crystallite surfaces of cellulose and disrupt the physical structure of cellulose [7,20]. Therefore, some studies have demonstrated the possibility of slow degradation of modified cellulose-based materials in vivo. The spongy structure of cellulose provides free entry for cells to invade and degrade very slowly; in rats, for example, the time scale is approximately 12 weeks [21]. With metabolically engineered Gluconacetobacter xylinus, cellulose can copolymerize with chitin. In vivo experiments have demonstrated that this copolymer is susceptible to both lysozyme and cellulase [22]. Cellulose sheets that were pre-irradiated became resorbable. An in vivo experiment revealed marked degradation at all time points, with the most rapid degradation occurring in the first 2 to 4 weeks [23].

In this study, we investigated three different methods to incorporate HA into TEMPO-oxidized BC (TBC) sponges by physical mixing, in situ formation and biomineralization. In these experiments, HA concentrations were identical in the three methods, and the only difference was the manner of HA nanoparticle incorporation. By assessing the pore architecture, load-bearing capability, structural anisotropy and degradability in vivo, we aimed to discover the correlation between microstructure and degradability. We wanted to explore whether it is possible for the modified BC/HA composite to satisfy competing mechanical and biological prerequisites to enable application in tissue engineering, especially in bone tissue defect healing.

2.Results and discussion

2.1 Morphological analyses of the composite sponges

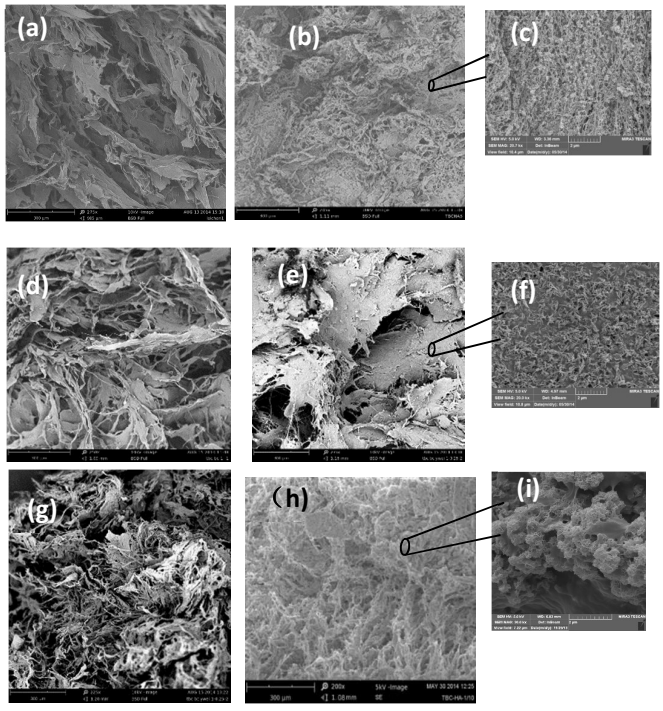

Fig. 1. Cross-sectional SEM images of sponges prepared under different conditions. Sponges prepared by in situ formation with a weight ratio of (a) TBC:HA=1:0.5; (b, c) TBC:HA=1:1. Sponges prepared by physical mixing with a weight ratio of (d) TBC:HA=1:0.5; (e, f) TBC:HA=1:1. Biomineralized TBC sponges

after 3 (g) and 5 (h, i) cycles of alternate soaking in calcium and phosphate solutions.

Table 1. Atomic Ca:P ratio from EDX for the various composites

method		Ca wt%	P wt%	Ca:P ratio
in situ formation	TBC:HA=1:0.5;	1.09	0.70	1.56
	TBC:HA=1:1;	1.05	0.63	1.67
physical mixing	TBC:HA=1:0.5	1.12	0.67	1.67
	TBC:HA=1:1	1.10	0.65	1.69
Biomineralization	3 cycles	2.93	1.45	2.0
	5 cylcels	1.08	0.47	2.3

Different preparation methods produced different results as described in Fig. 1, in which the calcium phosphate nanoparticles varied in size and morphology between the different TBC sponges. As for the in situ formation, pore walls appeared significantly more textured with increasing calcium phosphate ratio as shown in Fig 1a. Additionally, pore morphology tended to be irregular. High-magnification images indicated that spherical granules (40~60 nm) or agglomerates (100~300 nm) adhered to the nanofiber surface to form a looser network (Fig. 1c). However, the physical mixing method produced a different morphology; pores had become plugged as a result of the increased HA content (Fig. 1d,e). The enlarged cross section of the pore wall revealed that needle-like HA nanoparticles were inlaid in the surface layer of the dense sponge (Fig. 1f). The biomineralized sponges with higher calcium phosphate ratios exhibited similar rough and loose pore texture as the samples from in situ formation (Fig. 1h). However, the higher magnification images revealed that the calcium phosphate globules exhibited a honeycomb-like structure followed by further crystal agglomerative growth (Fig. 1i). Table1 showed the Ca:P ratio identified by EDX analysis for the various samples. This range of Ca:P ratios can indicate the forms of hydroxyapatite. In the present experiment, biomineralization preferred to form calcium-rich HA, while calcium deficient HA could be generated by precipitation on TBC in *in situ* formation system.

2.2 Structure and constituent analyses of the composite sponges

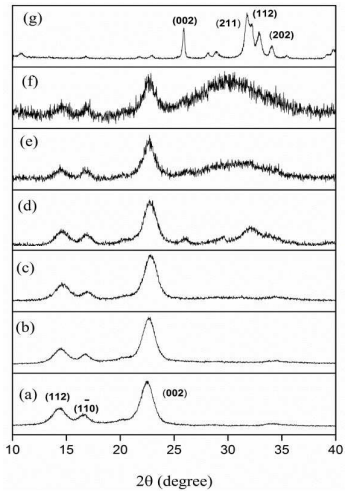

Fig.2. X-ray diffraction patterns of BC-HA composites. (a) TBC; (b) TBC:HA=1:0.5 (physical mixing); (c) TBC:HA=1:1 (physical mixing); (d) TBCCH 5 cycles (biomineralization); (e) TBC:HA=1:0.5 (in situ formation); (f) TBC:HA=1:1 (in situ formation); (g) pure HA.

X-ray diffraction (XRD) was performed on the dried native BC, HA and composite materials to determine how the composition method affected the crystallinity of the materials. The XRD pattern of TBC (Fig. 2a.) exhibited a typical crystalline structure of native cellulose as defined by sharp defined peaks at 14.4 and 22.5 values of 2θ that corresponded to the (112) and (002) planes. Fig. 2g exhibited characteristic and well-crystallized HA diffraction lines with a sharp peak (002) and split peaks corresponding to (211), (112) and (202). The composites prepared using physical mixing exhibited a similar pattern as that of TBC, regardless of the amount of HA used (Fig. 2b, c), suggesting that the composite produced by this method possessed higher crystallinity and higher density. No peaks corresponding to HA appeared in this composite. This unexpected result can be explained by the uneven distribution of pre-synthesized HA in composites. The pattern corresponding to the biomineralized samples (5 cycles) contained a broad peak at a 2θ value of approximately 32, indicating that TBC coexists with HA (Fig. 2d). Regarding the in situ formation method, the coarse curve pattern indicated poor crystallinity (Fig. 2e). As the HA ratio increased, the pattern tended to become amorphous (Fig. 2f).

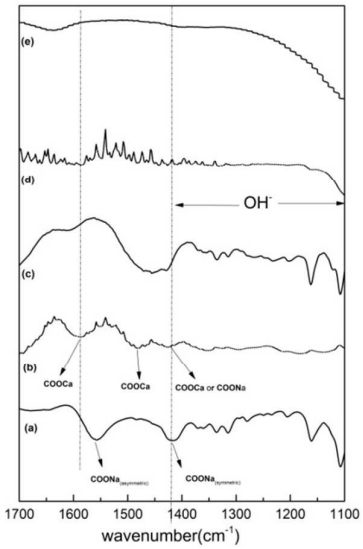

Fig. 3. ATR-FTIR spectra of various samples. (a) TBC; (b) TBC/HA prepared by in situ formation (TBCHA(1:1)); (c) TBC/HA prepared by physical mixing (TBCHA(1:1)); (d) TBC/HA prepared by biomineralization (5 cycles). (e)pure HA

The attenuated total reflection Fourier-Transform-infrared (ATR-FTIR) spectra of the various sponges are shown in Fig. 3. This study focused on a portion of the mid-infrared region from 1700 to 1100 cm^{-1} because the interaction of COO^- and Ca^{2+} plays a key role in determining the properties of complex sponges. When forming carboxylates, COOH group often shifts to lower bands. The two bands at 1556 and 1419 cm^{-1} were assigned to the asymmetric and symmetric vibration in TBC, respectively (Fig. 3a). Combination with calcium ions resulted in the appearance of some new peaks including the bands at 1479 and1592 cm^{-1} were assigned to the formation of complexes (COO-Ca) (Fig. 3b). The bands of (COO-Ca) and (COO-Na) often overlaps at 1419 cm^{-1}, disfavoring the differentiation between them. Moreover the bands of OH between 1362 to 1100 cm^{-1} began to fade. Physical mixing cause the disappearance of COO-Ca bands with appearance of a broad peak in the FTIR pattern (Fig. 3c), suggesting that the interactions between TBC and HA were much weaker in the in situ formation system. The electrostatic interaction often broadens the bands in the FTIR pattern [28], So it can be reasonably concluded that the ready-made HA nanoparticles electrostatically adsorbed on the nanofiber. Regarding biomineralized samples (Fig. 3d), the peak corresponding to COO^- is difficult to discern and was split into many small peaks, indicating that biomineralized TBC is more similar to BC. Unlike the in situ formation system, the engineered TBC sponges tended to shield COO^- inside the sponges, leading to decreased activity of the COO^- groups.

2.3 **Mechanical properties and structural anisotropy analysis of the composite sponges**

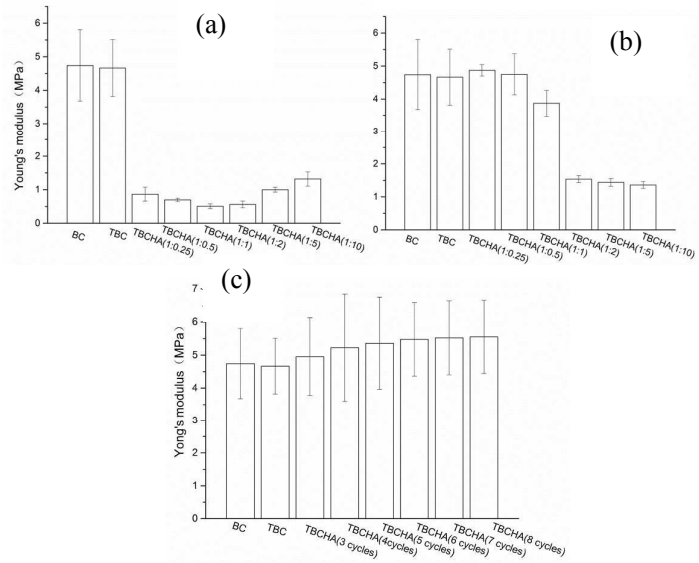

Fig. 4. Young's modulus of samples prepared by different methods. (a) In situ formation; (b) physical mixing; (c) biomineralization.

The mechanical properties of various samples are presented in Fig. 4. The data demonstrated that oxidation did not affect the Young's modulus of BC materials. However, the presence of HA in composite material had a completely different effect on the mechanical properties compared with various composite methods. The addition of HA nanoparticles by physical mixing increased the Young's modulus slightly at lower reinforcement levels (1:0.5 TBC:HA by weight in Fig. 4b). When the ratio was increased to 1:1, the Young's modulus decreased dramatically. As for the sponges prepared by in situ formation, the presence of HA caused an approximate 75% decrease in Young's modulus (Fig. 4a), suggesting that the formation of HA in the TBC network may weaken mechanical properties. A slight increase in Young's modulus could be observed in the mineralized sponges as shown in Fig. 4c. These findings indicate that the shape and crystallinity of the particles in the composite have a large influence on the mechanical properties.

The salient point in relationships between the mechanical properties of cellular solids is that the relative density dramatically influences the stiffness and the strength. The relative density is defined as the ratio between the density of the cellular solid to the density of the bulk material (ρ^*/ρ_s) [24]. Fig. 5 shows the relative density of different samples. The trends in relative density and elastic modulus were similar. The sponges prepared from pure BC had the highest relative density because of its dense microstructure. The sponges prepared by the in situ formation were characterized by loose

texture, high porosity, and thus low density. As the HA nanoparticle content in the mixing physical sponge increased, the density decreased, exhibited a minimum, and then increased. It is concluded that HA nanoparticles embedded in the network might decrease the hydrogen bonding between nanofibers, leading to a looser structure. However, the further addition of pre-synthesized HA with high crystallinity produced a conglomerate that potentially clogged some pores in the sponges. This observation could contribute to the increase in relative density after the minimum presented in Fig. 5. It is expected that the formation of apatite crystallites in the oxidized BC sponge could increase the density in the biomineralized material, which is in agreement with the findings of other studies. Under this condition, Ca^{2+} and PO_4^{3-} in the solution might mineralize and fill in the cracks in the TBC sponges, leading to an increase in density.

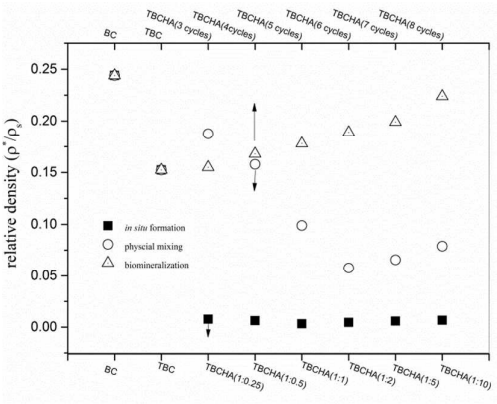

Fig. 5. The relative density of various sponges prepared by different methods

The models describing the mechanical behavior of open-foam solids are well developed [25-27]. The variation of Young's modulus of a porous solid with relative density is expressed in the form of equation (1):

$$\frac{E^*}{E_s} = C\left(\frac{\rho^*}{\rho_s}\right)^n \quad . \quad (1)$$

where E^* and E_s are the Young's modulus of the sponge and bulk material, respectively, and C is a constant which was found to be inversely proportional to pore regularity based on Oscar's experiment results [24]. An increased C value implies a more random arrangement of pores in sponges and greater anisotropy in the structure. The exponent n varies across different cellular systems.

The obtained results demonstrate that the mechanical properties of the sponges in this study are characterized by anomalous behavior arising from structural and material anisotropy [27]. However, the sponge mechanical behavior may be more complex than the idealized cellular solid, leading to a deviation from equation 1. Nevertheless, the composite sponges in these experiments can still be described quantitatively by modifying equation 1. Fig. 6 presents the variation of Young's modulus of the sponges with relative density. The relationship can be described by an expression of the form shown in Table 2.

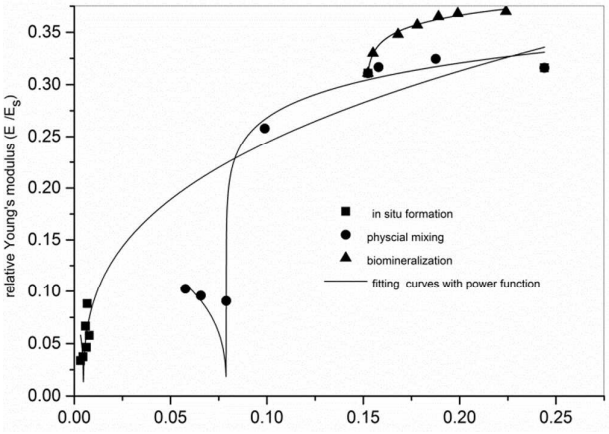

Fig. 6. Variation of Young's modulus of sponges with relative density for different composite methods.

Table 2. Equations and parameters predicting the relationship between relative density and Young's modulus.

Methods	Equations	Constant *C*	R^2
In situ formation	Y=0.549(X-0.004)0.3448	0.549	0.95913
Physical mixing	*Y=0.398(X-0.0789)0.3409	0.398	0.98900
Biomineralization	Y=0.4135(X-0.1516)0.04	0.4135	0.98801

*(X>0.0789)

The constant *C* was previously observed to correspond to regularity in the microstructure [27]. The calculated *C* values in Table 1 indicate that in situ formation leads to the most irregular composite sponge and that the sponges prepared by physical mixing exhibited less anisotropy compared with the other two methods.

2.4 *In vivo* degradation study

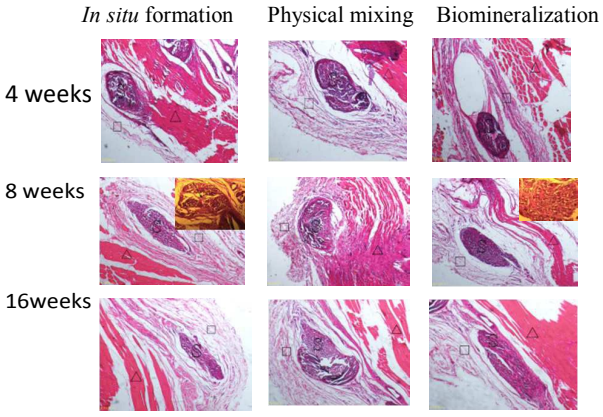

Fig. 7. HE staining of sections of implanted sponges at after 4, 8 and 16 weeks. 4× magnification. S denotes the sponges, △ denotes muscle tissue, □ denotes connective tissue and → denotes new capillaries. The sponges prepared by in situ formation (TBCHA (1:1)) 4 weeks (a), 8 weeks (d) and 16 weeks after implantation (i). Magnification inset (10×) depicts a new capillary vessel in the newly ingrown tissues (e). The sponges prepared by physical mixing (TBCHA (1:1)) 4 weeks (b), 8 weeks (f) and 16 weeks after implantation (j). The sponges prepared by biomineralization (TBCHA (5 cycles)) 4 weeks (c), 8 weeks (g) and 16 weeks after implantation (k). Magnification inset (10×) shows connective tissue surrounding the cracks (h).

In a typical tissue, nuclei and calcium are stained by hematoxylin and appear as blue dots, whereas the cytoplasm and extracellular matrix undergo varying degrees of pink staining. HE staining images revealed that none of the implants were infected after 4 weeks, suggesting that the sponges were well tolerated by the host animals for the duration of the experiment. However, the sponges failed to retain their cylindrical shape during the implantation period given mechanical stress on the implant.

Four weeks after implantation, the connective tissues entered the peripheral part of the sponges and filled **30**% of the cross-sectional area (Fig. 7a,b,c). Some cracks and fissures appeared in the central part of all implants. The connective tissues became denser after 8 weeks and formed a network throughout the sponges (Fig. 7d,g) except the physical mixing sample in which only 50% of the area was filled (Fig. 7f). It is very clear that the growth of granulation tissue surrounded the material fragments (Fig. 7d) in the sponges of in situ formation and the biomineralized sponges (Fig. 7g). However, the capillaries appeared in the peripheral part of the sponge (Fig. 7e), suggesting that the granulation tissue gradually matured. The sponges were completely filled with mature granulation tissue at week 16 post-surgery in the samples prepared by in situ formation and biomineralization (Fig. 7i,k). Particularly for the sponges of in situ formation, some fragments were enclosed by condensed connective tissue as shown in Fig. 7i. Moreover, a slight retraction appeared to occur throughout the sample. As for the biomineralized sponges, the framework was loose and a large fissure could be observed in the central part (Fig. 7k). Instead of being filled completely, the implants prepared by physical mixing contained fibrillar fragments in the peripheral part and a few splintered materials in the central zone (Fig. 7j).

Cellulose and its derivatives are considered non-degradable in vivo because humans lack cellulase. Any tissue present at 8 weeks in the sponges of in situ formation consisted of vascularized tissue. It can be concluded that the sponges might have degraded slightly in vivo. To support this conclusion and quantify degradation, GPC was used to determine the molecular weight and degree of polymerization of various samples.

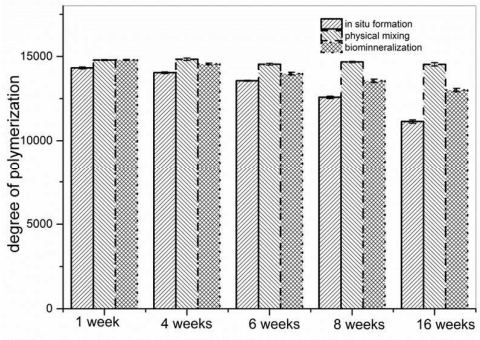

Fig. 8. Changes in degree of polymerization (DP_V) of various sponges in vivo.

The DPV of polymerized sponges decreased from 14,320 to 11,140 within 16 weeks (Fig. 8), indicating that the sponges experienced some degradation in vivo. The change is not dramatic but is still detectable. No obvious changes were detectable in the other two sponges. These results are consistent with the HE analysis.

3.Discussion

Numerous studies have been reported regarding the combination of calcium phosphate with BC. In the present experiment, the properties of composites directly depend on how HA was applied, which is subsequently determined by HA-BC interface formation. To theoretically explain this phenomenon, we provide schematic illustrations of interaction mechanisms between nanofiber and HA nanoparticles (Fig. 9 and 10). The carboxylic groups on the modified BC reduce the hydrogen force between the -OH groups and consequently the adhesion between BC nanofibers (Fig. 9b). Carboxylic groups

prefer to form chelated complexes with metal ions that are kinetically and thermodynamically more stable. Regarding the in situ formation system, carboxyl groups can engage in binding to Ca^{2+} as shown in Fig. 10c. Based on the ART-FTIR pattern (Fig. 3), it can be deduced that TBC/HA complexes prepared by in situ formation formed mainly via coordinate bonding between Ca^{2+} and COO^- at the nanofiber surface as shown in Fig. 10c. The successive addition of PO_4^{3-} and OH^- produced a precipitate of HA nanoparticles on the TBC nanofiber surface, leading to bulk fiber swelling (Fig. 9e). The loose spongy structure with amorphous HA often causes a decrease in tensile strength and relative density. With the physical mixing method, the composite materials were obtained by mixing pre-synthesized HA and BC aqueous suspensions (Fig. 9f). In this case, the COO^- groups are bound to HA nanoparticles by strong electrostatic interaction (Fig. 10d) [17], which represents a relatively simple type of interaction between the cellulose and the HA surface. In contrast to the composites obtained by in situ formation, the pre-synthesized HA nanoparticles exhibited increased crystallinity and were embedded in the sponge wall as shown in Fig. 1f, forming a relatively dense microstructure that exhibited higher tensile strength.

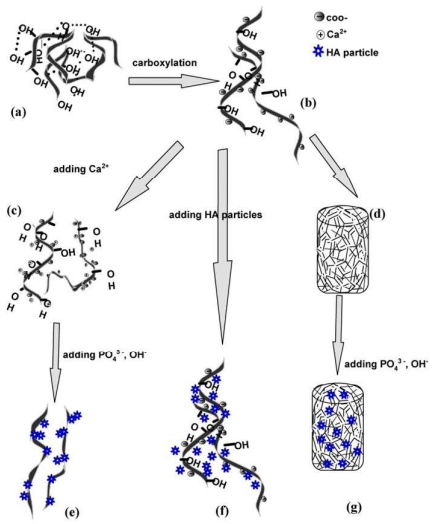

Fig. 9. Schematic illustration of HA nanoparticle precipitation process in three types of systems. (a) The nanofiber becomes entangled as a result of extensive hydrogen bonding. (b) The nanofiber is stretched by surface carboxylation. In the in situ formation system, Ca^{2+} chelates with surface COO^- (c). Further addition of PO_4^{3-} and OH^- forms HA on the surface, causing a looser and swollen structure (e). Addition of ready-made HA nanoparticles, which become electrostatically adsorbed on the nanofiber, produces a dense structure (f). (d) The prepared TBC sponge. (g) HA nanoparticles mineralized within the sponges.

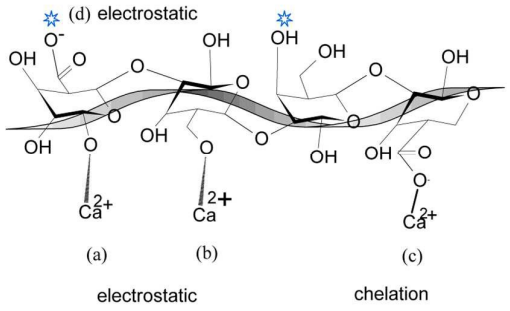

Fig. 10. Various interactions between Ca^{2+} and a TBC nanofiber. (a) Ca^{2+} electrostatically bonds with OH groups on the cellulose surface. (b) Ca^{2+} electrostatically bonds with unreacted OH6 groups at the C6 position. (c) Chelation between Ca^{2+} and COO^-. (d) HA nanoparticles electrostatically adhere to the nanofiber surface.

The biomineralization in the engineered sponges differs from the others because the nanofibers are in closer contact, leading to relatively strong hydrogen bonding. The biomineralized sponges are therefore much stiffer than the post-prepared samples, as confirmed in the tensile strength experiments. With additional soaking cycles, HA is deposited to the point of possibly blocking channels in the sponges (Fig. 9 g), resulting in increased relative density. Unlike the in situ formation system in which bulk fibers are swollen and more exposed carboxyl groups can engage in binding with Ca^{2+}, the interaction between TBC and HA during biomineralization is more complex. The ready-made sponges tend to decrease the accessibility of COO^-. Thus, at least two types of interactions responsible for the combination between HA nanoparticles and TBC are noted. One is Ca^{2+}-COO^- chelation, which can be detected by the shift in the COO- band (Fig. 10c). Another is electrostatic attraction, which often plays the main role in structure formation during the conventional biomineralization process (Fig. 10b) [17].

In the present study, the microstructure plays a large influence on the in vivo degradation of cellulose-based materials. Scanning electron microscopy (SEM) allows partial examination of this microstructure. To completely describe the sponges prepared by different methods, the anisotropy of the cellular solids was analyzed. The anisotropy consists of structural anisotropy and material anisotropy. However, only structural anisotropy was considered in our experiments through measurement of the constant *C* in equation 1. Based on the calculations, the microstructure of the sponges

prepared by in situ formation exhibited the greatest anisotropy and the highest *C* value, whereas physical mixing methods produced a more regular microstructure and the smallest *C* value. The diversity of the interactions between HA and TBC might be responsible for the anisotropy. With in situ formation, three types of interactions might exist. Individual fibers were bound to HA nanoparticles predominantly by chelation, as schematized in Fig. 10c. When the amount of surface carboxylated groups was reduced, the excess Ca^{2+}, PO_4^{3-} and OH^- promoted HA crystal growth as usual. Furthermore, the stretched nanofiber exposed more unmodified OH groups on the fiber surface, providing more opportunities for hydrogen bonding between the O atoms of OH groups and Ca^{2+}. This finding is consistent with previous reports and as schematized in Fig. 10a [15]. Numerous types of chemical reactions are possible in this system. Regarding the physical mixing system, HA was added in the form of engineered nanoparticles with higher crystallinity that are unlikely to grow continuously. As the neutral nanoparticles, HA has a very limited opportunity to participate in reactions beyond electrostatic reactions (Fig. 10d). The diversity of chemical bonding in the biomineralization system is an intermediate state between the other two. As discussed above, the ready-made sponges tend to shield COO^-, leading to a decrease in the activity with ions. Ca^{2+}-COO^- chelation and electrostatics are the dominant forms of interaction in the system.

Through in vivo experiments, the in situ formed sponges were filled with granulation tissue fastest, whereas only the peripheral part was covered by connective tissue in sponges obtained by physical mixing 16 weeks after surgery. Many published studies have reported that lower relative density and looser microstructure are often favorable for producing a higher rate of connective tissue ingrowth [29,30]. This finding is consistent with our observations of the polymerized sponges. However, it is not universal for the biomineralized sponges, which exhibit a higher relative density but an increased speed of connective tissue ingrowth compared with sponges made by physical mixing. The present experiment demonstrated a high correlation between anisotropy and the ingrowth of new tissues in the sponges. It is worth noting that natural cellular materials, such as bone, wood and coral, which have evolved to meet the challenges of their environments via efficient mechanisms, are generally strongly anisotropic [31]. It can be concluded that the sponges with higher anisotropy mimicked natural bone morphology and exhibited better biocompatibility, enabling new tissue ingrowth. Therefore, the biomineralized sponges exhibited an increased rate of connective tissue ingrowth. Furthermore, the ingrowth of new tissues in the sponges is an essential prerequisite of biodegradation in vivo. Although humans lack cellulase, modified cellulose materials are susceptible to lysozymes and hydrolytic enzymes [22]. In the present experiment, the in situ formed TBC/CH composite degraded slowly in vivo. Degradation of cellulose generally involves the cleavage of a β(1→4) bond depending on which most often occur in the amorphous parts of the cellulose. Therefore, the cellulose material with lower degree of crystallinity is more unstable in vivo. Although the question of what type of enzyme caused the degradation of TBC/HA composite in the present experiment has not yet been fully answered, the reduced crystallinity exhibited by the modified composite might be responsible for the degradation. Carboxylation and precipitated HA nanoparticles on the individual nanofibers formed by in situ formation reduce the density of hydrogen bonds, enhancing accessibility to enzymes. The sponges made by the physical mixing method exhibited the highest crystallinity as shown by XRD and were not degraded in vivo. Compared with the other two sponges prepared by biomineralization and in situ formation, the nanofibers in the engineered sponges held together more tightly so that the individual molecules were less accessible to enzymes. Degradation of the sponges obtained by in situ formation was likely a combination of low crystallinity and high structural anisotropy.

4.Experimental

4.1 Materials

$(NH_4)_2HPO_4$ (AR grade), $Ca(NO_3)_2$ (analytical reagent (AR) grade), $NH_3{\cdot}H_2O$ (AR grade), TEMPO (AR grade), NaClO solution (AR grade, 13.4% available chlorine), and $NaClO_2$ (AR grade) were purchased from Sigma-Aldrich (USA) and were used without further purification. The water used in these experiments was purified by deionized reverse-osmosis water. Bacterial cellulose (BC) pellets (donated by Guangyu Biotechnology Co., Ltd., China) were stored at 4°C. Male Sprague-Dawley rats (specific-pathogen free (SPF) grade, 10 to 13 weeks of age) were purchased from The First Affiliated Hospital of Guangzhou Medical university. All animal procedures followed the “Guide for the care and use of laboratory animals (National Research Council, 1996)”. All animal experiments were conducted under the permits of ethical review committees of Peking University Shenzhen institute(Longshi Jiang, Aihua Wu, Nan Fang, Tao Huang , Li Na, Zhen zheng and Shuaiyan Wang). Sprague–Dawley rats which were individually housed and provided water and soy-bean based food (irradiated pellets, Guangzhou Medical University) at all times. Housing rooms were maintained on a 12/12-h light/dark cycle (9 am–9pm) at 25 ± 1°C (mean ± SE) and 60–65% humidity. The room was ventilated 8~12times/day.

4.2 Preparation of TEMPO-mediated oxidized bacterial cellulose (TBC)

TBC (TEMPO-oxidized BC) was prepared via TEMPO oxidation as reported previously [7,20]. To obtain TBC in the TEMPO/NaClO/$NaClO_2$ system, 1 g of BC suspension in 300 mL of phosphate buffer (0.05 M, pH 6.86) was obtained using a homogenizer (IKAT25, Germany) with the speed of 25 000 rpm at room temperature. TEMPO (0.1 mmol/g BC) and $NaClO_2$ (17 mmol/g BC) were added to the resulting suspension. NaClO (2

mL) was diluted in 100 mL of the phosphate buffer solution, and the resulting mixture was immediately added to the suspension. The suspension was then sealed and magnetically stirred at 65°C for 30 h. The products were washed four times via centrifugation and then lyophilized for further analysis.

4.3 Preparation of TBC/HA composites (TBCHA) sponges

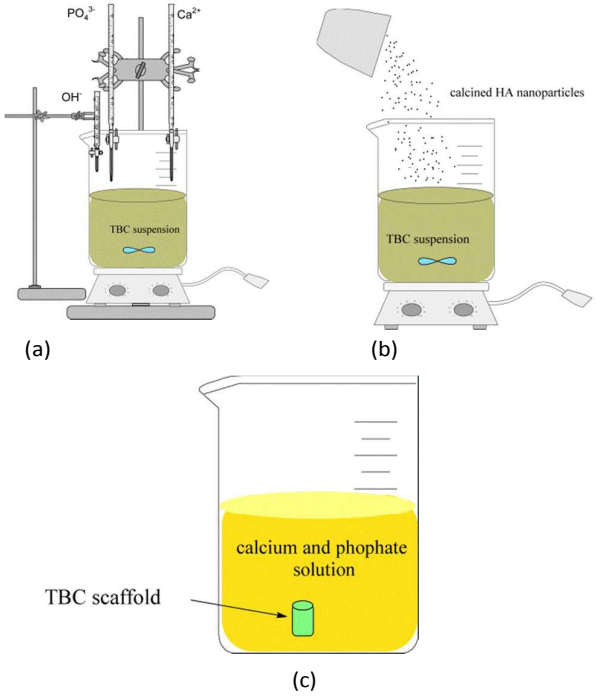

Fig. 11. Schematic diagram depicting the preparation of HA/TBC composites using three different methods: (a) in situ formation, (b) physical mixing, and (c) biomineralization.

For in situ formation, $(NH_4)_2HPO_4$ and $Ca(NO_3)_2$ were first dissolved in distilled water to form 0.5 M and 1 M aqueous solutions, respectively. TBC suspensions were produced in parallel by the homogenization of freeze-dried TBC in deionized water at room temperature using a homogenizer (IKA T25, Germany) operated at 25,000 rpm. The $(NH_4)_2HPO_4$ and $Ca(NO_3)_2$ aqueous solution were then slowly dropped into an intensively stirred TBC suspension with different concentrations at room temperature, simultaneously keeping the pH value above 11 with ammonia as shown in Fig. 11a. The mixture was degassed in a vacuum desiccator for 1 hour to remove air bubbles, transferred into polytetrafluoroethylene (PTFE) molds, and frozen at -20°C. The samples then were freeze-dried for 48 h in a vacuum of 0.05 mbar, thus removing the ice crystals by sublimation and leaving porous solid sponges.

In the physical mixing method, needle-like HA nanoparticles with a mean length of 500 nm were precipitated by a hydrothermal reaction using 1 M $Ca(NO_3)_2$ solution and 0.5 M $(NH_4)_2HPO_4$ solution in a sealed oven at 120°C for 12 h. The resulting white precipitate was washed thoroughly with distilled water and oven-dried at approximately 50°C. TBC suspensions were produced as described above. HA nanoparticles were then added to the TBC suspension under vigorous stirring as shown in Fig. 11b. The subsequent treatment was the same as for the in situ formation method.

For the biomineralization process as shown in Fig.11c, 1 M $CaCl_2$ and 0.5 M NaH_2PO_4 were prepared. Cylindrical TBC sponges 10 mm in height and 5 mm in diameter were alternatively soaked in the calcium and phosphate solutions at 37°C for 30 min with reciprocal shaking at 50 strokes/min. The sponges were rinsed thoroughly with distilled water between each soaking cycle. A total of 3 to 8 soaking cycles were performed. The final samples were oven-dried at 37°C for 3 days.

4.4 In vivo degradation experiment

Dry sponges with dry weight of 17.12 ± 3.7 mg were cut into cylinders (5 mm diameter, 5 mm height) and sterilized with epoxyethane. The sponges were implanted into 45 male SD rats (180~260 g, SPF grade), with 3 rats in each group. Pentobarbital sodium (30 mg/kg body weight) was administered prior to surgery. Taking the spine as the central axis, two symmetric incisions were made in the back of each rat. The sponges were inserted into each wound, which were subsequently closed using 6-0 silk sutures. After periods of 1, 4, 6, 8 and 16 weeks, the original wounds were reopened, and the sponges and surrounding tissue were removed. The harvested samples were immediately fixed in 4% formaldehyde in phosphate-buffered saline (PBS) at room temperature and embedded in paraffin to cut tissue sections. The sections were stained with hematoxylin and eosin (HE) and were observed under an optical microscope (Zeiss, Germany)

4.5 Characterization

Dried samples 10 mm in height and 5 mm in diameter were loaded under uniaxial compression at a rate of 0.01 mm/s to ~75% strain using a universal materials testing machine (Instron, USA). Compression was continuous until the sponge was completely flattened (100% strain). The Young's modulus for compression was calculated using the graphical value output from the MTS software. The compressive modulus was calculated by linear least squares regression using the segment of the apparent stress-strain curve.

ATR-FTIR spectroscopy was performed using a Nicolet 6700 spectrometer (Thermo, USA) with a resolution of 4 cm^{-1}; the samples were scanned from 1700 to 1100 cm^{-1}.

The crystallinity of BC and oxidized BC were analyzed by X-ray diffraction (XRD) on a Bruker AXS, D8 Advance Diffractometer with CuKa radiation (γ=1.54 Å) at 40 kV and 40 mA.

Morphological characterization was conducted using scanning electron microscopy (PhenomTM, Netherlands). The device was equipped with EDX spectrometer for elemental microanalysis. The samples were prepared by fracturing them in liquid nitrogen. Fragments were adhered to a cupreous stub by double-faced adhesive tape and coated with gold before analysis. The EDX spectra were collected for at least 30s each at 20kv

The sponge density was determined according to the ASTM D1505 method.

Degradation in vivo was quantified by the change of molecular weight using gel permeation chromatography (GPC; Viscotek GPC/SEC 270max, Malvern, UK). The samples were washed carefully with PBS to remove the tissue. The TBC/CH composites were dissolved in a NaOH:urea:water solution (7:12:81 by weight) at -15°C, obtaining a clear solution. The solution was filtered using 1 μ m filters (Gelman) before injection into the GPC system. The following parameters were used for GPC measurements: flow rate, 1.00 mL /min^{-1}; column, CLM3021@35°C (A6000M, General Mixed Aq 300 × 8.0 mm); injection volume, 200 μ L; run time, 20 min. Data evaluation was performed with a PEO standard and OmniSEC 5.0 software. The degree of polymerization (DP_v) was calculated by dividing the molecular weight of repeated units of TBC/HA as follows:

$$DP_V = \frac{M_n}{1181} \qquad (2)$$

where M_n is the number-average molar mass of the samples as determined by GPC.

5.Conclusions

HA is often combined with various polymers given its biocompatibility. Individual synthesis methods have been published in many previous reports. In the present study, we compared several methods side by side. The function of HA in this study depended on the integration technique. The composites formed with Ca^{2+} and well-dispersed nanofibers often broke the extensive hydrogen-bound structure of the cellulose network, thus decreasing the mechanical properties, degree of crystallinity and relative density. Under these conditions, the interaction between HA and TBC assumed various forms, including chelation and electrostatic reactions, leading to strong anisotropy in the microstructure. When HA was added in the form of engineered nanoparticles with high crystallinity, the combination of TBC and HA was relatively straightforward. Electrostatic attraction was the major contribution to the energy of interaction between cellulose and the HA surface. Compared to the sponges prepared by in situ formation, this type of sponge had a denser and more irregular structure. As for biomineralized sponges, the ready-made sponges saturated the available hydrogen bonding in the network, leading to the highest tensile strength and relative density. The dense structure prevented the COO^- from being fully exposed; therefore, the chelation of Ca^{2+} and COO^- was no longer the dominant reaction in the system. Furthermore, the various addition methods of HA led to various forms of interaction between the cellulose and HA, causing diversity in the structural anisotropy of the sponges. Although the in vivo degradability of BC is limited, its modified counterpart can potentially degrade in vivo if the network density is varied. The modified BC-based sponges with loose and swollen microstructure exhibited noticeable degradation in this study within 16 weeks. The amount of new tissue ingrowth in the implants was consistently correlated with the size, shape and internal structure of the implants. Furthermore, we believe that the structural anisotropy and the speed of granulation ingrowth were strongly interdependent. In the present study, the structures with increased anisotropy exhibited faster formation of granulation tissue and hence faster degradation in vivo. Suggested further research includes an investigation of the enzymatic mechanisms that contribute to molecular cellulose decomposition. Additionally, future observation periods need to be sufficiently long to achieve total disappearance of the cellulose sponge within subcutaneous tissue. In any case, for the present study, it is noted that the ingrowth of granulation tissue provided favorable conditions for degradation. The GPC technique confirmed the slow degradation of sponges possessing the highest structural anisotropy and fastest granulation ingrowth. It is expected that polymerized sponges will be most useful when they exhibit lower density, loose texture and porosity, all of which promote tissue ingrowth. Comparing the sponges in the biomineralization and physical mixing systems, the denser sponges with increased relative density resulted in faster granulation ingrowth. This unexpected result supports the conclusion that the structural anisotropy of sponges plays an important role in granulation ingrowth and degradation. BC features many excellent mechanical properties and is biocompatible, but its non-degradability in vivo restricts its development in tissue engineering. Here, we have established that it is possible to modify the degradability of cellulose-based material by altering the microstructure.

conflict of interest

The authors declare no competing financial interest

Acknowledgements

This research was supported by the Major State Basic Research Development Program (973 project no. 2012CB933600).
Key Projects in the National Science & Technology Pillar Program during the Twelfth Five-year Plan Period(2012BAI17B02, 2012BAI18B00).Science and technology

research Foundation of Shenzhen Bureau of science and technology & information（JCYJ20140419114548513）

References

1 S. Teixeira, M.A. Rodriguez, P. Pena, A.H. De Aza, S. De Aza, M.P. Ferraza and F.J. Monteiro, Mat. Sci .Eng. C , 2009, 29, 1510.
2 N.T. Carpena, Y.K. Min and B.T Lee, ASAIO .J, 2015, 61, 78.
3 X.F.Song, F.G.Ling, L.L.Ma, C.G. Yang and X. S. Chen, Comp. Sci. Tech, 2013, 79, 8.
4 M.V. Cabañas, J. Peña, J. Román ,C. Ramírez-Santillán, M.C. Matesanz, M.J. Feito, M.T.Portolés and M. Vallet-Regí, , Mat. Chem. Phy, 2014, 144, 409.
5 K.Maji and S. Dasgupta , Trans .Ind. Ceram. Soc, 2014, 73,110.
6 J. M. Rajwade, K. M. Paknikar and J. V. Kumbhar，Appl. Micro. Biotech, 2015, 99,2491.
7 C.Lai ,S.J.Zhang ,X.C. C and L.Y. Sheng，Cellulose,2014, 21, 2757.
8 H. Yano, J. Sugiyama, A.N. Nakagaito, M. Nogi, T. Matsuura, M. Hikita and K. Handa,. Adv. Mat, 2005, 17 ,153.
9 S.Eftekhari, I.E. Sawi, Z. S.Bagheri, G.Turcotte and H.Bougherara , Mat. Sci. Eng. C, 2014, 39 ,120.
10 A. S. Hutchens, J.Woodward, B.R. Evans and H.M. O'neil, Composite Material. U.S. Patent application No. 20040096509.
11 G.M. de Olyveira, M.L. dos Santos, L.M.M. Costa, P.B.Daltro, P. Basmaji, G.D. Daltro and A.C.Guastaldi, J. Biom. Tiss. Eng, 2014, 4,536.
12 S.Shi, S.Y.Chen, X.Zhang, W.Shen, X.Li, W.L. Hu and H.p. Wang, , J. Chem. Tech. Biotech, 2009, 84, 285.
13 S.Chalal, S.J.H.Fathima and M.B.M.Yusoff, Bio-Med. Mat.Eng,2014,24, 799.
14 A.Kumar,Y.S.Negi,V. Choudhary,N. and K.Bhardwaj, Cellulose, 2014, 21,3409.
15 X. X. Fan, T. T. Zhang, Z. T. Zhao, H. H. Ren, Q. Y. Zhang, Y. G. Yan and G.Y. Lv, J. Appl. Poly. Sci. 2013, 129,595.
16 N Barbani, G.D. Guerra, C. Cristallini, P. Urciuoli, R.Avvisati, A. Sala and E.Rosellini, J . Mat. Sci. 2012, 23,51.
17 D. A. Tolmachev and N. V. Lukasheva,Langmuir, 2012, 28,13473.
18 H.L Luo; G. Y Xiong, C. Zhan, d.y. Li, Y . Zhu, R. S . Guo and Y. z. Wan, Mat. Sci. E .C,2015, 49,52.
19 M. González;E. Hernández;J. A. Ascencio;F. Pacheco;S. Pacheco and R. Rodríguez, J. Mat. Chem., 2003, 13,2948.
20 C.Lai , S.J.Zhang, L.Y. Sheng, S.B.Liao ,T.F. Xi and Z.X. Zhang ， Coll. Poly. Sci, 2013, 291,2985.
21 M.Märtson, J.Viljantoa,T.Hurmea, P. Laippalac and P.Saukkob, Biomaterial, 1999, 20,1989.
22 V.Yadav, B.J. Paniliatis, H.Shi, K. Lee, P.Cebe and D. L. Kaplan, Appl. Envir, 2010,676,257.
23 W.Czaja, D. Kyryliouk, C. A. DePaula and D.D. Buechte, J. Appl .Polym. Sci. 2014, 131,39995.
24 O.E. Sotomayor and H.V. Tippur, Act .Mater,2014, 78,301.
25 B.A Harley, J.H. Leung and E.C .Silva, L.J. Gibson, Act .Mater,2007,463, 3.
26 E. O. Sotomayor and H.V. Tippur, Act .Mater, 2014, 78,301.
27 O.E. Sotomayor and H. V. Tippur, Int. J .Sol. S, 2014, 51,3776.
28 Q. Zhang, Q. F. Zhang, S. B. Zhang and S.h. Li, J.Memb. Sci, 2010, 354,23
29 H. Ahrem, D. Pretzel, M .Endres, D .Conrad, J. Courseau, H .Müller, R .Jaeger,C .Kaps, D.O. Klemm and R.W. Kinne, Act. Biom, 2014, 10,1341.
30 M. Mrtson, J. Viljanto, P. Laippala and P. Saukko, Eur. Surg. Re,1998, 30,41.
31 L. J. Gibson , M.F. Ashby, Anisotropy of Foam Properties, in: L. J. Gibson , M.F. Ashby (Eds.),Cellular Solids: Structure and Properties second edition, Cambridge University Press., Cambridge , 1997,pp.257-277.…

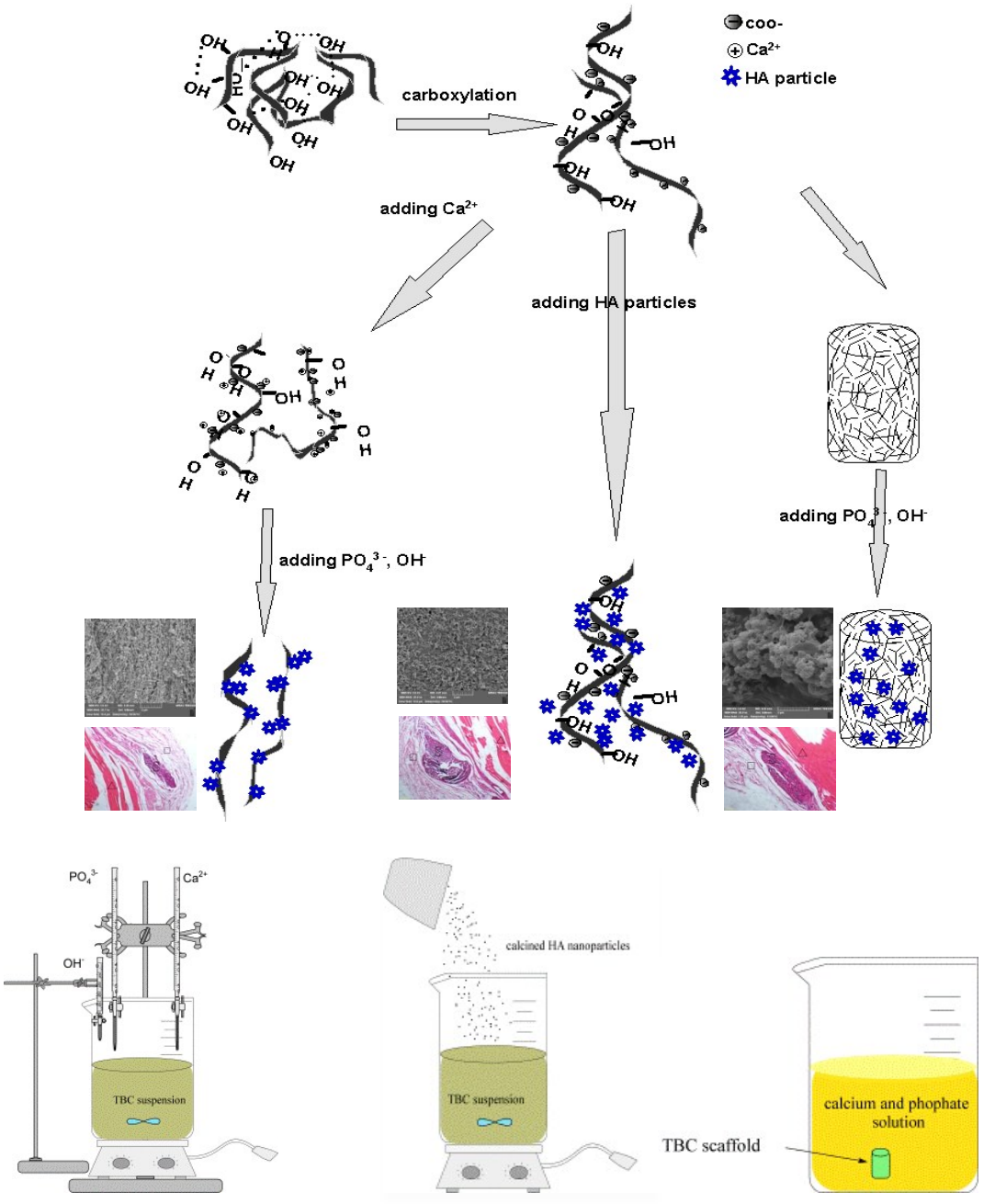

The interaction between the nanofibers of bacterial cellulose and hydroxyapatite has an extensive influence on the microstructure and the macroscopic properties of this type of composite and that the structural anisotropy and the speed of granulation ingrowth are strongly interdependent.